ISSN (Print) 1226-1750
ISSN (Online) 2233-6656
Journal of Magnetics 25(2), 313-317 (2020) https://doi.org/10.4283/JMAG.2020.25.2.313

Coexistence of Ferromagnetism and Paramagnetism in Graphene with Boron-vacancy Complex

S. H. Rhim*

Department of Physics, University of Ulsan, Ulsan, 44610, Republic of Korea

(Received 10 March 2020, Received in final form 12 June 2020, Accepted 25 June 2020)

Defect induced magnetism in a single layer graphene with Boron-vacancy complex is studied using highly precise *ab initio* full-potential linearized augmented plane wave (FLAPW) method. From energetics, it is most stable when Boron and vacancy are the nearest neighbor. Furthermore, we propose both paramagnetic and magnetic states, with negligible energy difference, can coexist in defected graphene. The *k* resolved band structure reveals that the magnetism is mainly from different occupation of very localized impurity bands. Moreover, calculated STM image associated with defect is presented to provide some hint in experimental verifications.

Keywords : graphene, magnetism, Boron doping

1. Introduction

Graphene, a hexagonal lattice with two Carbon atoms in unit cell, has attracted in recent years for its intriguing physics as well as potential for future device applications [1-3]. As a building block for various Carbon allotropes such as Carbon nanotubes, graphite, and fullerene, the electronic structure of graphene is intensively and extensively studied. In exploration for device applications, understanding of graphene with doping and its resultant properties is very important. Carbon allotropes have been interesting for many years exhibiting various properties such as half-metallicity [4, 5] and even superconductivity with an external electric field [6]. Boron (Nitrogen) has one electron less (more) than Carbon with virtually the same atomic radius, can serve hole (electron) doping to carbon systems. Boron doped Carbon systems have been interesting for many years [7]: superconductivity was reported in diamond [8, 9], cubic Silicon [10], and graphene with an external electric field. Further, it was proposed as a good candidate for material for hydrogen storage [11], and its stability against oxidation was also discussed [12].

On the other hand, magnetism in carbon related materials has fascinated in many ways, where defects play a crucial role. In previous studies, it has been shown that defect in carbon systems is very common phenomenon [13, 14] and that associated magnetism is intrinsic [13, 15, 16]. It was reported that a single vacancy in graphite give a localized magnetic moment of order 0.5-1.0 μ_B. Further, studies on graphene fragments [17-19] and graphene nanoribbon [4, 5] extended understanding magnetism in carbon systems, where in both cases, edge states contribute to long-range ferromagnetic ordering. In particular, graphene nanoribbon exhibits half-metallicity with an applied electric field [5], which opened a new gate to carbon-based spintronics. In this sense, study of magnetic properties of carbon with doping would be very interesting.

Among dopants to graphene, Boron is less studied than Nitrogen or Hydrogen. Moreover, Nitrogen doping in graphene is shown not necessarily to enhance magnetism [20], thus investigating magnetism with hole doping would be worthwhile. Thus, in this work the interplay between vacancy and Boron substitutional dopant (hereafter B/v) is investigated using first-principles *ab initio* density functional theory [21] calculations. Formation energies (*FE*), electronic structure, and magnetism of B/v are presented. Furthermore, the coexistence of magnetic and non-magnetic phases in B/v is proposed.

2. Methods of Calculations

The highly precise all-electron full-potential linearized

*Corresponding author: Tel: +82-52-259-2325
Fax: +82-52-259-1693, e-mail: sonny@ulsan.ac.kr

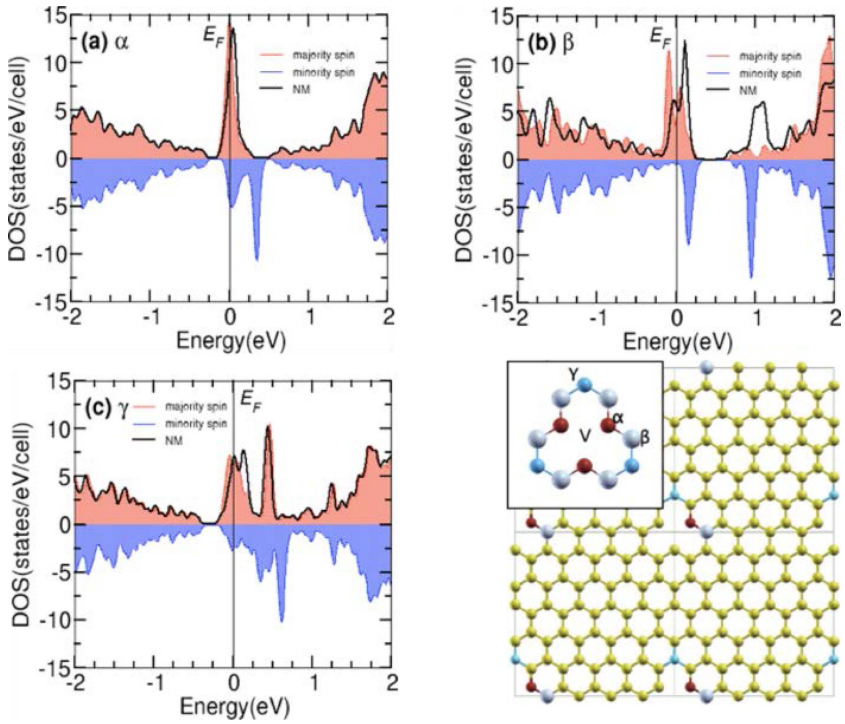

Fig. 1. (Color online) Density of state plots of both magnetic and nonmagnetic state for (a) α, (b) β, and (c) γ, respectively. DOS of nonmagnetic (NM) states are shown in black line, those of magnetic states are shown in red (blue) shaded area for majority (minority) spin. Fermi level is set to energy zero. Geometry for calculations in 5 × 6 cell with one vacancy at the origin, where four cells are shown here. Inset: Possible B positions, α, β, and γ, are denoted with letters and balls in color of red (dark), larger grey (larger bright), and light blue (bright), respectively. Vacancy is denoted as character V at the center of inset.

augmented plane wave (FLAPW) [22, 23] is employed for *ab initio* density functional calculations, as implemented in *flair* [24]. Experimental lattice constant of graphene (2.46 Å) is used throughout calculations, and geometry optimization performed by fully relaxing atomic positions with force criteria 0.05 eV/Å. Cutoff energy of the plane-wave basis is 12.25 Ry and that of potential representation is 144 Ry. Muffin-tin radii of 1.25 a_B are used for both C and B. For the exchange-correlation potential, generalized gradient approximation (GGA) by Perdew, Burke, Ernzerhof (PBE91) [25] is used, and core states are treated fully relativistically. The geometry in considerations are shown in Fig. 1: α is when B and vacancy is the closest, β the second closest, and γ the third, respectively, where "5×6" graphene lattice of rectangular shape is used. Brillouin zone sampling in Monkhorst-Pack scheme [26] is done with 10 × 10 × 2 mesh to include *K* point in "5×6" rectangular unit cell. All possible cases for three configurations are shown in inset of Fig. 1, where symmetrically equivalent atoms for each configuration are also shown. As rectangular unit cell is used in calculations, band zone unfolding into convention graphene hexagonal cell is applied in *k* resolved band plots [27].

3. Results and Discussions

Formation energy (*FE*) of each configuration is evaluated by using $FE = E_C + E_P - (E_V + E_B)$, where E_C, E_P, E_V, and E_B are the total energy of each configuration, the perfect 5 × 6 graphene cell, the cell with one vacancy, and boron substituted cell without vacancy, respectively. In all cases, *FE* of both non-magnetic and magnetic solutions are taken into account, which are summarized in Table 1: The α is the lowest in *FE*, which indicates that Boron and vacancy tend to be close to each other. The difference of

Table 1. *FE* (in eV) of B/v complex of both magnetic and non-magnetic solutions for each configuration. Total magnetic moment (MM, in μ_B) for magnetic solutions are shown in parentheses. The formation energy difference between magnetic and nonmagnetic states (ΔE_{diff}) for each configuration (in meV) is listed in the last column.

	Magnetic (MM)	Nonmagnetic	ΔE_{diff} (meV)
α	–3.69 (0.66)	–3.68	–4.92
β	–2.341 (1.04)	–2.27	–39.99
γ	–2.22 (0.54)	–2.20	–17.45

FEs between magnetic and non-magnetic states for each configuration (ΔE_{diff}) is less than 40 meV in all cases, where magnetic states are slightly more stable. The small ΔE_{diff} implies a possible coexistence of magnetic and non-magnetic states in B/v complex near or above room temperature, of which detailed analysis follows later.

Density of states (DOS) plots are given in Fig. 1: (a) α, (b) β, and (c) γ, respectively. Both magnetic and non-magnetic states are plotted. The difference between magnetic and non-magnetic is evident near E_F, while two phases exhibit similar DOS in other energy range. A common feature in all cases is large DOS peaks nearby E_F are due to impurity bands mostly from vacancy. DOS peaks of non-magnetic states are further split into the majority and minority spin. From DOS, it is obvious that DOS peaks in non-magnetic state results in magnetic instability, while large DOS peaks in magnetic states implies magnetism in B/v complex is of localized character, in contrast to itinerant magnetism.

To investigate strong possibility of the coexistence of magnetic and non-magnetic states from small ΔE_{diff}, fixed spin moment (FSM) calculation is employed and we follow the analysis given in Ref. [28]. Within FSM approach, each spin channel has its own Fermi energy, whose separation indicates the magnetic field (H) necessary to maintain the given spin moment. Plots of fixed moment (**M**) *vs* applied field strength (H) are presented in Fig. 2. At very low moments, all cases show Curie-Weiss paramagnetic behavior. Zero-field ($H = 0$) solutions are denoted in blue circles for each case, which implies re-entrant behavior of magnetism. Broad region of negative field for moments is that of magnetic instability. Further self-consistent calculations are performed with converged densities from FSM calculations. When fixed moment constraints are removed, solutions are driven to magnetic ones, whose magnetic moments agree with the normal self-consistent spin-resolved calculations. This confirms that both magnetic and non-magnetic solutions are stable in B/v complex. As shown in Table 1, small energy difference (4.92 meV) between magnetic and non-magnetic solutions in α is further investigated. Magnetic solution is reexamined with several broadening values which corresponds to temperature in k point sampling.

The k resolved surface bands of the α case is presented in Fig. 3: (a) nonmagnetic solution. Boron substitution simply acts as a hole doping, whereas vacancy induces gap opening at K as well as forming impurity states. Band structure of magnetic configuration of α is shown for both majority and minority spins in Fig. 3(b) and (c), respec-

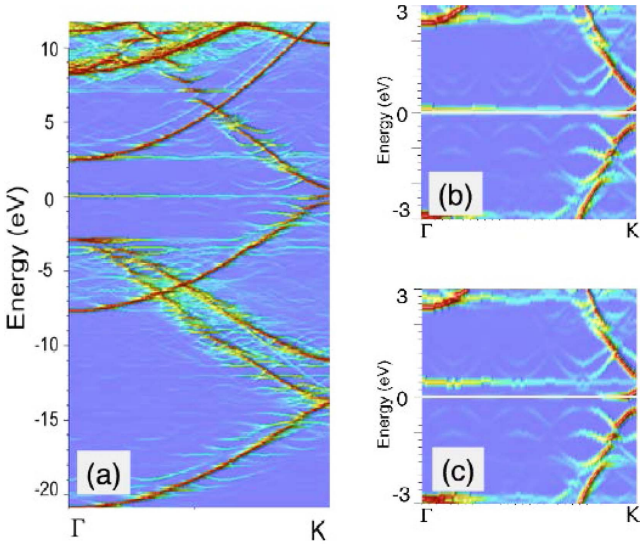

Fig. 3. (Color online) k resolved band structure plots of α (a) nonmagnetic, and closer view of magnetic states of (b) majority and (c) minority spin. Fermi level is taken as zero energy and shown in white line.

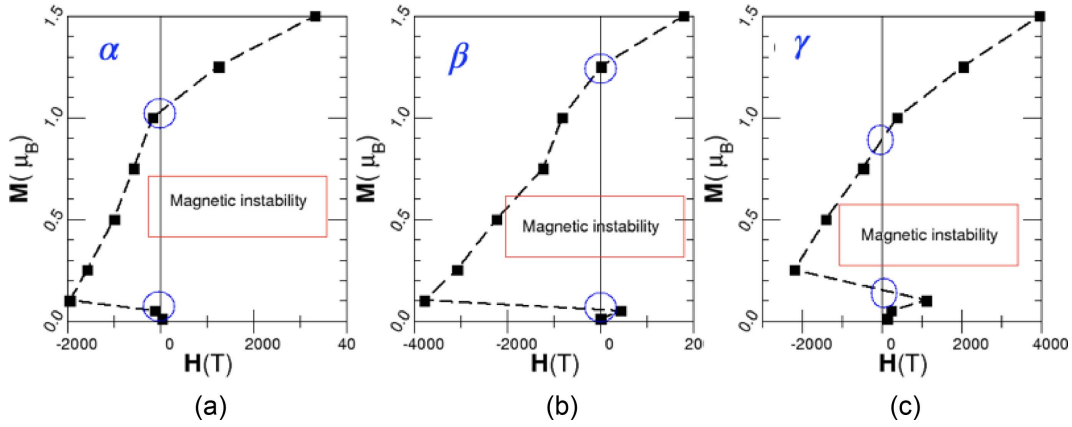

Fig. 2. (Color online) Calculated applied field (H) vs magnetic moment (M) for B/v for each configuration: (a) α, (b) β, and (c) γ. Zero field solutions ($H = 0$) are denoted by blue circles and magnetic instability region is presented in each case.

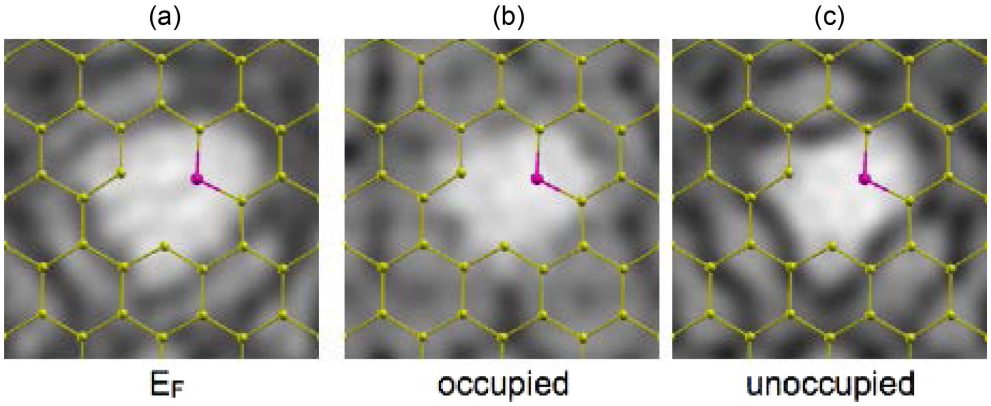

Fig. 4. (Color online) Calculated STM plot of α, for state (a) around E_F, (b) occupied (–0.5 eV – E_F), and (c) unoccupied (E_F –0.5 eV), respectively. Red (yellow) ball represents Boron (Carbon) atom. Density of $10^{-6}\ e/a_B^3$ is chosen for iso-density, where contours correspond to height from the surface having the reference density.

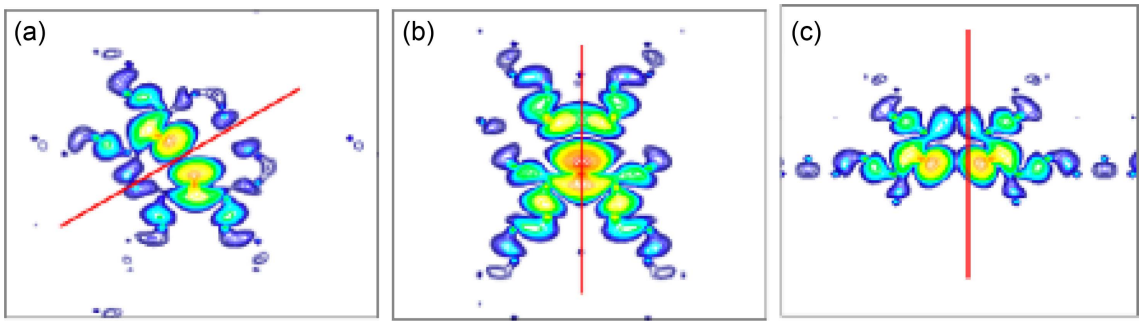

Fig. 5. (Color online) Spin density plots of magnetic state for each configuration with four unit cells for better visibility. (a) α, (b) β, and (c) γ, respectively. Solid lines represent the mirror plane connecting vacancy-Boron with two-fold symmetry. Starting spin density is $10^{-7}\ e/a_B^3$ with subsequent lines increasing by a factor 1.25.

tively. Magnetism in Boron-vacancy defected graphene is mainly due to the difference of occupation of each spin channel, which is the same for β and γ with slight changes in the position of impurity bands.

Figure 4 shows iso-density plots of α for various bias voltages: (a) around E_F, (b) occupied [–0.5 eV – E_F], and (c) unoccupied states [E_F – 0.5 eV], respectively. Here, we emphasize that the iso-density plots are theoretical simulation of scanning tunneling microscopy (STM), which are contour plots of the same charge densities different from conventional charge density plots. Here, charge density of $10^{-6}\ e/a_B^3$ is chosen, where e is the elementary charge, and a_B is the Bohr radius. Heights from the surface is taken for contour plots, which corresponds to the constant-current mode of STM.

Finally, spin density plots are presented in Fig. 5, where four unit cells are taken for comprehensibility. As seen in Fig. 5, in all cases, spin densities are highly localized near the vacancy. The distribution of spin densities reflects two-fold symmetry where associating mirror planes are denoted in lines. This contrasts to the single-vacancy case where spin density exhibits three-fold symmetry. Furthermore, the spin density plot strongly implies the magnetism in B/v complex exhibits highly localized feature. In this work, we argue that more than simple defects is necessary to realize long-range magnetism.

4. Summary

In summary, the coexistence of magnetic and non-magnetic phases in B/v is studied. Boron and vacancy tend to be close to each other from formation energies as in nitrogen-vacancy case [20]. DOS plots show that magnetism in B/v is of localized character as evidenced from large DOS peak at E_F. Possible instability shown in large DOS peaks at E_F is not removed in magnetic phases, indicating it is of defect states. Moreover, the energy difference of magnetic and non-magnetic phases (ΔE_{diff}) are very small, which would lead to the coexistence of both magnetic and non-magnetic phases, noting that doping or vacancy generation in experiment is commonly accompanied in very high temperature. Further, FSM vs

applied field analysis clearly reveals that both magnetic and non-magnetic solutions are stable. The localized feature of magnetism in B/v is well demonstrated in spin density plots.

Acknowledgement

This work was supported by the 2017 Research Fund of University of Ulsan. Author is grateful to Michael Weinert, Lian Li, and Arthur J. Freeman for fruitful discussions.

References

[1] K. S. Novoselov, A. K. Geim, S. V. Morozov, D. Jiang, M. I. Katsnelson, I. V. Grigorieva, S. V. Dubonos, and A. A. Firsov, Nature **438**, 197 (2005).
[2] Y. Zhang, Y.-W. Tan, H. L. Stormer, and P. Kim, Nature **438**, 201 (2005).
[3] A. H. C. Neto, F. Guinea, N. M. R. Peres, K. S. Novoselov, and A. K. Geim, Rev. Mod. Phys. **81**, 109 (2009).
[4] Y.-W. Son, M. L. Cohen, and S. G. Louie, Phys. Rev. Lett. **97**, 216803 (2006).
[5] Y.-W. Son, M. L. Cohen, and S. G. Louie, Nature **444**, 347 (2006).
[6] K. Nakamura, S. H. Rhim, A. Sugiyama, K. Sano, T. Akiyama, T. Ito, M. Weinert, and A. J. Freeman, Phys. Rev. B **87**, 214506 (2013).
[7] O. Stephan, P. M. Ajayan, C. Colliex, P. Redlich, J. M. Lambert, P. Bernier, and P. Lefin, Science **266**, 1683 (1994).
[8] E. A. Ekimov, A. Sidorov, E. D. Bauer, N. N. Mel'nik, N. J. Curro, J. D. Thompson, and S. M. Stishov, Nature **428**, 542 (2004).
[9] Y. Takano, M. Nagao, I. Sakaguchi, M. Tachiki, T. Hatano, K. Kobayashi, H. Umezawa, and H. Kawarada, Appl. Phys. Lett. **85**, 2851 (2004).
[10] E. Bustarret, C. Marcenat, P. Achatz, J. Kačmarčik, F. Lévy, A. Huxley, L. Ortéga, E. Bourgeios, X. Blase, D. Débarre, and J. Boulmer, Nature **444**, 465 (2006).
[11] Y. G. Zhou, X. T. Zu, F. Gao, J. L. Nie, and H. Y. Xiao, J. Appl. Phys. **105**, 014309 (2009).
[12] N. Park and S. Moon, J. Kor. Phys. Soc. **53**, 2024 (2008).
[13] A. Hashimoto, K. Suenaga, A. Gloter, K. Urita, and S. Iijima, Nature **430**, 870 (2004).
[14] P. O. Lehtinen, A. S. Foster, A. Ayuela, A. Krasheninnikov, K. Nordlund, and R. M. Niminen, Phys. Rev. Lett. **91**, 017202 (2003).
[15] J. M. D. Coey, M. Venkatesan, C. B. Fitzgerald, A. P. Douvalis, and I. S. Sanders, Nature **420**, 156 (2002).
[16] P. Esquinazi, A. Setzer, R. Höhne, C. Semmelhack, Y. Kopelevich, D. Spemann, T. Butz, B. Kohlstrunk, and M. Lösche, Phys. Rev. B **66**, 024429 (2002).
[17] H. Lee, N. Park, Y. W. Son, S. Han, and J. Yu, Chem. Phys. Lett. **398**, 207 (2004).
[18] H. Lee, Y. W. Son, N. Park, S. Han, and J. Yu, Phys. Rev. B **72**, 174431 (2005).
[19] H. Lee, Y. Miyamoto, and J. Yu, Phys. Rev. B **79**, 121404(R) (2009).
[20] S. H. Rhim, Y. Qi, G. F. Sun, M. Weinert, and L. Li, Appl. Phys. Lett. **100**, 233119 (2011).
[21] P. Hohenberg and W. Kohn, Phys. Rev. **136**, B864 (1964).
[22] E. Wimmer, H. Krakauer, M. Weinert, and A. Freeman, Phys. Rev. B **24**, 864 (1981).
[23] H. Jansen and A. J. Freeman, Phys. Rev. B **30**, 561 (1984).
[24] M. Weinert, http://www.uwm.edu/?weinert/flair.html.
[25] J. P. Perdew, K. Burke, and M. Ernzerhof, Phys. Rev. Lett. **77**, 3865 (1996).
[26] H. J. Monkhorst and J. D. Pack, Phys. Rev. B **13**, 5188 (1976).
[27] Y. Qi, S. H. Rhim, Guofeng Sun, M. Weinert, and L. Li, Phys. Rev. Lett. **105**, 085502 (2010).
[28] Yu. S. Dedkov, C. Laubschat, S. Khmelevskyi, J. Redinger, P. Mohn, and M. Weinert, Phys. Rev. Lett. **99**, 047204 (2007).